*Exploration Geophysics (2004) **35**, 33–40*
Butsuri-Tansa (Vol. 57, No. 1)
Mulli-Tamsa (Vol. 7, No. 1)

Numerical and laboratory investigations of electrical resistance tomography for environmental monitoring

Tania Dhu Graham Heinson

Key Words: Electrical resistance tomography, ERT, environmental monitoring, free-convective flow, salinity plumes, numerical modelling, laboratory modelling

ABSTRACT

Numerical and laboratory studies have been conducted to test the ability of Electrical Resistance Tomography – a technique used to map the electrical resistivity of the subsurface – to delineate contaminant plumes. Two-dimensional numerical models were created to investigate survey design and resolution. Optimal survey design consisted of both downhole and surface electrode sites. Resolution models revealed that while the bulk fluid flow could be outlined, small-scale fingering effects could not be delineated. Laboratory experiments were conducted in a narrow glass tank to validate theoretical models. A visual comparison of fluid flow with ERT images also showed that, while the bulk fluid flow could be seen in most instances, fine-scale effects were indeterminate.

INTRODUCTION

The ability to identify and map the transport of soluble contaminants is important in many situations. Hazardous-waste disposal sites, landfills, and saline disposal basins are examples of areas where the escape of leachates can lead to serious environmental problems (Simmons et al., 2002). In areas where contamination has occurred, the extent of contamination needs to be delineated and any changes in this distribution during remediation operations need to be mapped (Daily et al., 1995).

Conventional environmental monitoring consists of point sampling, normally via an intrusive process such as grid drilling. This is an expensive and labour-intensive technique that only provides information on effects at the sample site (Zhou, 1996; Johnson et al., 1996; Granato and Smith, 1999). In situations such as landfills, intrusive sampling can be dangerous and may not be representative of the complex groundwater environment (Ogilvy et al., 1999, Chambers et al., 1999). This has led to the assessment of alternative techniques, such as geophysical methods, for environmental monitoring applications (Bevc and Morrison, 1991).

Many contaminants decrease pore water resistivity and hence may be detected by electrical geophysical techniques. Electrical resistance tomography offers one such method for characterising groundwater contamination patterns. It is a technique that estimates the resistivity distribution within a subsurface volume based on numerous discrete voltage and current measurements (Daily and Owen, 1991).

Co-operative Centre for Landscapes Environment and Mineral Exploration
School of Earth and Environmental Sciences
University of Adelaide
Adelaide
SA, Australia 5005
Phone: 08 8303 5959
Facsimile: 08 8303 4347
E-mail: tania.dhu@adelaide.edu.au

Presented at the 16th ASEG Geophysical Conference & Exhibition, February, 2003.
Revised paper received 15 December, 2003.

Electrical resistance tomography (or ERT) has previously been applied for both site characterisation and monitoring of remediation programs in various situations including:

- Characterisation of landfill and hazardous waste disposal sites (Ogilvy et al., 1999)
- Remediation of dense non-aqueous phase liquids (Newmark et al., 1998)
- Bioremediation of hydrocarbons (Atekwana et al., 2002)
- Gasoline and saline leak characterisation (Bevc and Morrison, 1991).

This paper investigates the capabilities of ERT using numerical modelling and laboratory-based testing. The conclusions are based firstly on theoretical models which were created to explore optimal electrode arrays and spatial resolution, followed by a series of laboratory tests that examined the ability of ERT methods to image free convective flow in a highly constrained environment.

FREE CONVECTIVE FLOW

Many groundwater contaminants have contrasting density to in-situ pore fluids and groundwater. For example, waste disposal sites, hazardous material injection zones, agricultural activities, and accidental spills can all produce leachates that are denser than in-situ pore fluids and meteoric groundwater (Simmons et al., 2002). Density contrasts lead to the formation of gravitational instabilities (free convection), resulting in the development of lobe-shaped perturbations, initially at the base of the plume and then within the body of the plume (Simmons et al., 2002; Oostrom et al., 1992). If lateral transport (advection) is small, free convection leads to a greater quantity of solute being able to mix more quickly and spread further than can be achieved by diffusional transport mechanisms. For example, convection processes in saline basins may cause brines to mix over distances several orders of magnitude greater than due to diffusion alone (Simmons and Narayan, 1998). Investigations into the effects of the density gradient of fluids in groundwater systems such as seawater intrusion, high-level radioactive waste disposal, and infiltration of leachates from waste disposal sites have also highlighted the importance of density-driven flow as a transport mechanism (Huyakorn et al., 1987; Hassanizadeh and Leijnse, 1988; Frind, 1982).

ELECTRICAL RESISTANCE TOMOGRAPHY

Electrical resistance tomography can be used to elucidate the resistivity distribution within a volume, based on the measurement of numerous electrical potentials that arise due to the application of a stationary current within the same volume. The tomographic images created can be either two-dimensional surfaces or three-dimensional volumes that reflect resistivity contrasts existing within the medium. Subsurface resistivity is highly dependent upon fluid content (Nobes, 1996) and therefore in clean sandy environments, such images of resistivity distribution may reflect subsurface flow. We note that this is not always the case in reality, because of the presence of clays and other conducting minerals.

However, such distributions are static and therefore are not so important in the time-lapse ERT demonstrated in this paper.

A known current is transmitted from a point source into a conductive subsurface, and the resultant potentials are observed at other locations on the surface and within boreholes if available. The potential difference between any two points can then be calculated (Figure 1a). The position of current injection is then changed incrementally and the mapping process is repeated until data have been gathered at many combinations of current transmission and voltage measurement sites (Figure 1b).

Figure 1 is for a pole–pole electrode configuration, but other methods including bipole–pole and bipole-bipole electrodes can also be used. Pole–pole surveys are achieved by placing the current sink and reference potential electrodes a large distance away from the current source and potential measurement site, in order to approximate infinite separation (Figure 2a). Bipole–pole surveys are achieved by positioning only one electrode (either current sink or potential reference) a large distance away from the other electrodes to approximate an infinite separation (Figure 2b). Bipole–bipole surveys have all electrodes within the zone of influence (Figure 2c). Different configurations have different sensitivities, which are considered by Zhou and Greenhalgh (1999) through investigations of the Fréchet derivatives.

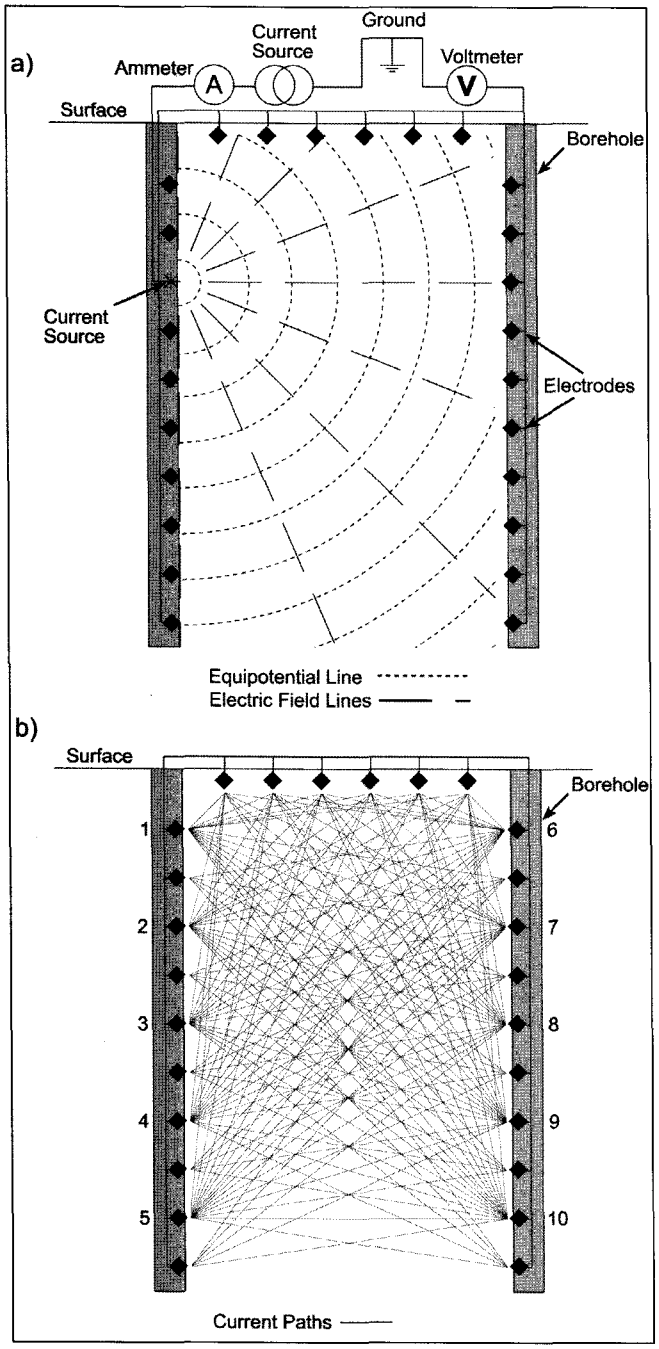

Fig. 1(a). An ERT system transmits a known current at a fixed point and records the potential at other electrodes sites. This process is then repeated, sequentially rotating through current transmission sites (numbered 1 to 10) and recording the associated potentials. (b) Schematic current pathways.

Once current and potential measurements are collected, the potential differences are normalized with respect to current to calculate a "transfer resistance" via Ohm's law:

$$V = I * R \qquad R = \frac{V}{I}, \tag{1}$$

where R is resistance (Ohms), V is voltage (Volts) and I is current (Amps).

Many transfer resistance measurements are used to estimate the resistivity distribution within the volume. The inversion of transfer resistance data to resistivity distribution is a non-linear problem, as noted by Tripp et al. (1984) and LaBrecque and Ward (1988).

Mathematically, calculating the resistivity distribution is dependent on solving Poisson's equation (equation 2) subject to the Neumann boundary conditions (equation 3).

$$-\nabla \cdot \left(\rho^{-1} \nabla \Psi\right) = F \tag{2}$$

$$\rho^{-1}(s)\eta \cdot \nabla \Psi = J(s) \tag{3}$$

In these equations ρ is the resistivity of the area to be imaged, Ψ is the electrical potential, F is the current source distribution within the area, s is the area to be imaged and $J(s)$ is the current density. The use of these boundary conditions requires that the boundary is a sufficiently large distance away from the current sources and sinks that the gradients of the fields are constant at the boundaries, and this was determined numerically for the laboratory experiment configurations. The aim of a reconstruction algorithm is to estimate

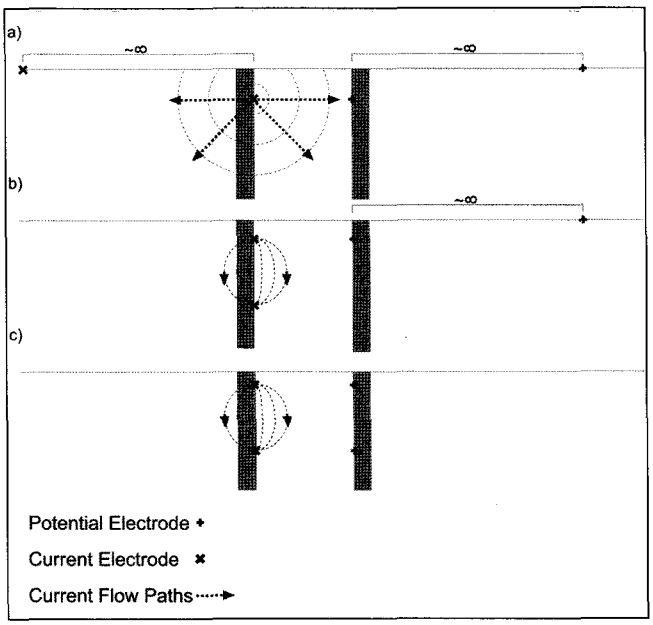

Fig. 2. Pole-pole (a), bipole–pole, (b) and bipole–bipole electrode arrays can all be used for electrical resistance tomography.

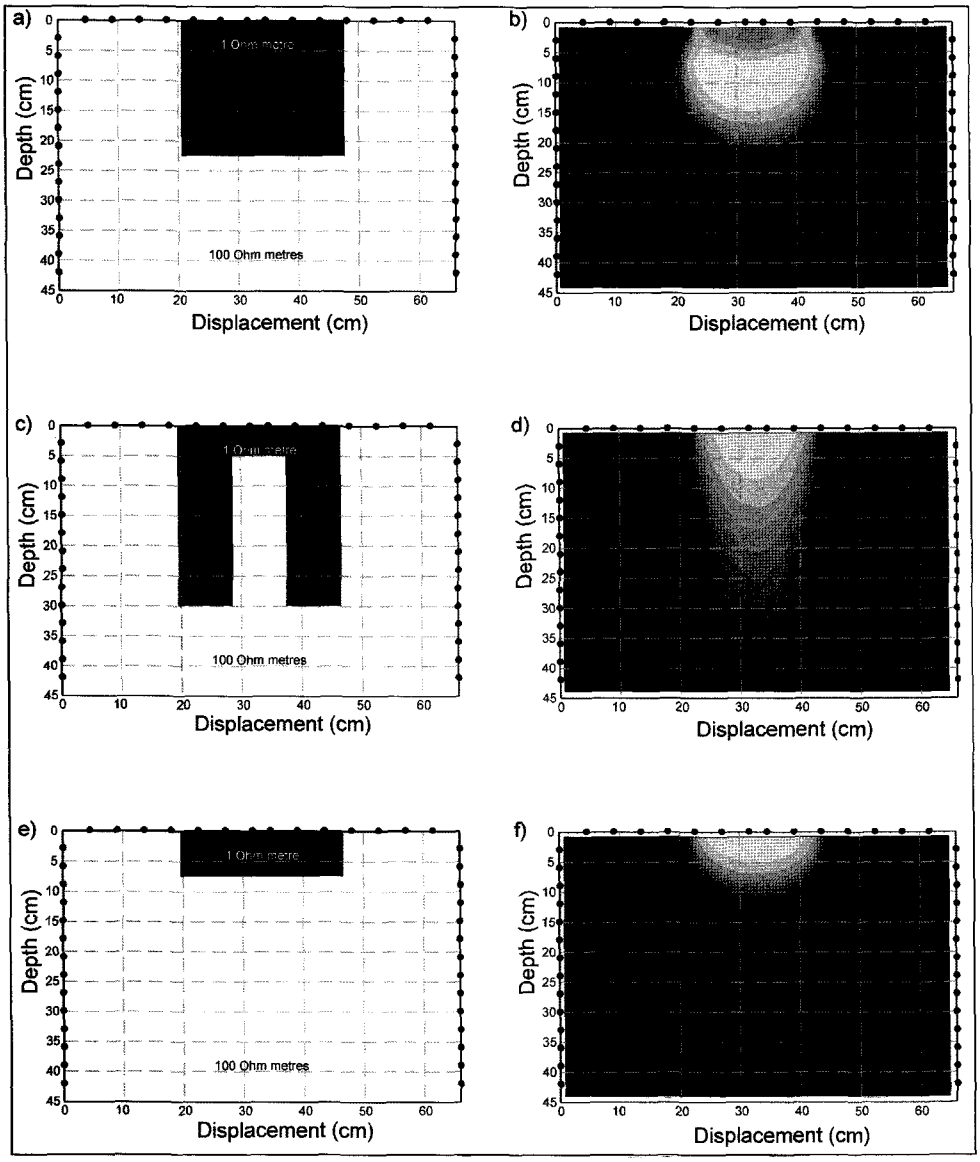

Fig. 3. Numerical modelling of three different plume configurations and their associated ERT images. Forty-two evenly spaced electrodes were used; fourteen in each borehole and fourteen on the surface, marked with black dots. Starting models (on left) show conductive bodies of 1Om in a resistive half space of 100 W.m. In the inverse models (on right), light colours are conductive, dark colours resistive. A simple conductive rectangle (3a), simulating a saline plume, was reconstructed successfully (3b). A more complicated conductive body (3c), imitating free convective fingering, was resolved but with no recovery of complexities (3d). A small simple rectangle (3e), approximating an early time saline plume, was well resolved (3f).

the spatial variation of resistivity, based on multiple measurements of the electrical potential and applied current (Daily and Owen, 1991). There exist various studies of reconstruction algorithms that address this problem (LaBrecque, 1989; LaBrecque et al., 1996b; Daily and Owen, 1991), but in this study the commercial codes RES2DINV (Loke and Barker, 1996a, b) and RES2D (Zhou and Greenhalgh, 1997, 1999, 2000) were used.

NUMERICAL MODELLING

Various theoretical models were constructed to investigate resolution limitations and capabilities of ERT, and optimisation of electrode positions. Forward models were created using RES2D (Zhou and Greenhalgh, 1997, 1999 and 2000) and inverted using RES2DINV (Loke and Baker, 1996a, b). The inversion algorithm uses a minimum structure approach, constraining the lateral and vertical gradient of resistivity weighted against a misfit function. The weighting function is determined numerically as an optimal trade-off between minimum misfit and modelled roughness. The inversion model mesh used is the same as the forward model mesh, and block sizes are approximately equal to the dimensions of the separations between electrode positions. All numerical models used the same finite element mesh with 1320 nodes, 44 elements horizontally and 30 elements vertically, with nodes spaced 1.5 units apart. In the inversions discussed here, the forward modelled data were treated as being exact (with no Gaussian noise added) as the optimal case. Introduction of typical levels of Gaussian noise (1–5%) would reduce the resolution of structure.

Plume Resolution

The nature of ERT surveying requires that a large number of measurements be made in order to solve the non-linear inversion problem required to estimate the resistivity distribution (Slater et al., 1997). Resolution is dependent on the number of electrodes, borehole spacing, electrode separation, and the subsurface resistivity structure (Ramirez et al., 1993). Spatial resolution can be increased by adding more electrodes and decreasing electrode separation. However, the time it takes to complete one measurement (all electrode combinations) increases with the square of the number of electrodes, so increasing spatial resolution is only achieved with associated decreases in temporal resolution (LaBrecque et al., 1996b). Daily and Owen (1991) stated that the number of linearly independent transfer resistances recorded in an ERT survey with n electrodes is $n(n\text{-}3)/2$. This implies that an increase in the number of electrodes, to improve resolution, will also significantly increase the computation time required to construct the tomographic image.

Initially, models of a simple rectangular plume shape (such as would occur with a saline plume) with a resistance of 1 Ω.m in a half-space of 100 Ω.m were created. The contrast between the plume and half-space resistivities is within the bounds of those measured in other studies that consider the interaction between fresh and saline water in the subsurface (Barrett et al., 2002; Frohlich and Urish, 2002). Forty-two electrodes were simulated in a pole–pole configuration, in a combination of borehole-to-borehole and borehole-to-surface arrangements, with the aim of testing the ability of ERT to image conductive contaminant plumes of 1 Ω.m with various dimensions in a 100 Ω.m half-space (Figures 3a, c, and e).

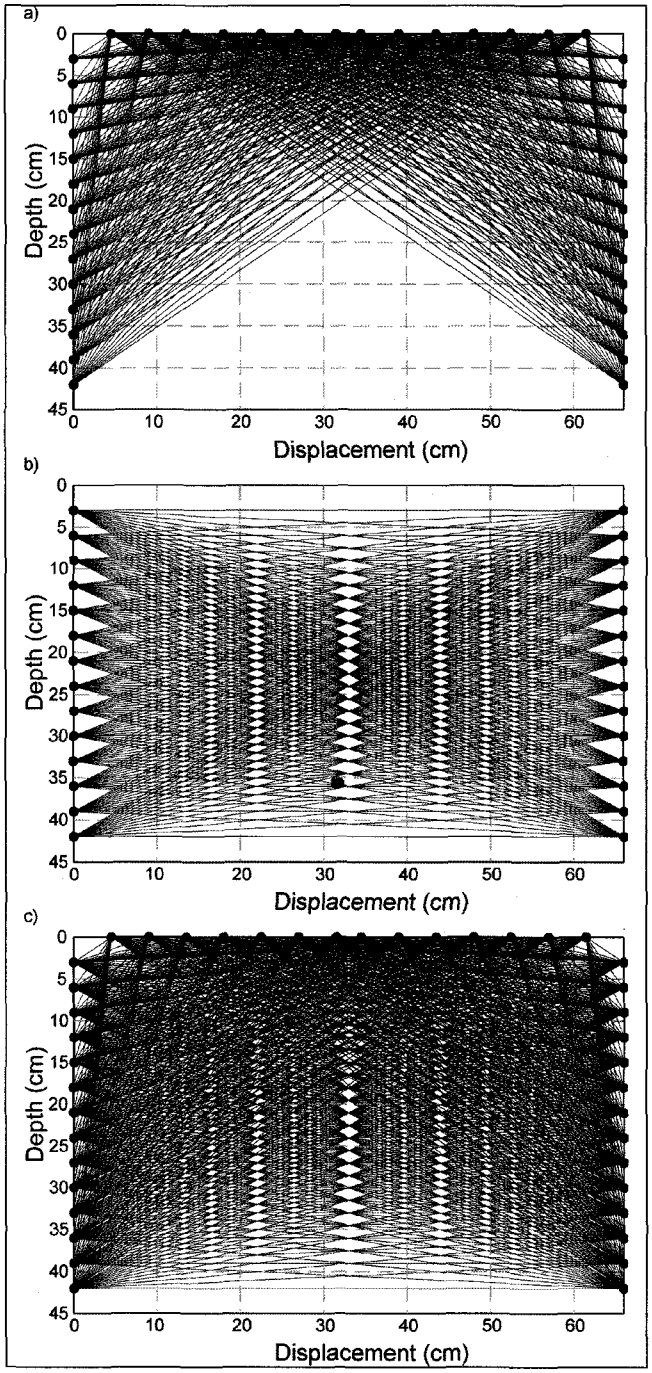

Fig. 4. Thin lines represent the expected ray paths for 42 electrodes in a half space.
(a) Borehole to surface measurements show good shallow coverage but no coverage with depth.
(b) Borehole to borehole measurements show good coverage at edges but poor coverage in the centre.
(c) All combinations gives the best coverage, but still loses some coverage towards the centre with depth.

Figure 3b shows the inversion of the simple conductive plume in Figure 3a. The image clearly delineates the plume, with reasonable resolution. A small conductive artefact below the base of the plume was also present in the image, but was orders of magnitude less conductive than the main plume body. The attempt to delineate fingering displayed in Figure 3c was not successful. The resultant inversion (Figure 3d) merged the two fingers into one, showing a plume that is narrower then the input model and also longer. A small plume (Figure 3e) was successfully imaged, but a conductive artefact was again present at the same location as in Figure 3b. The ability to image small and medium plumes indicates that ERT can be successful in mapping changes of plume shape during its development. The failure of the technique to image the fingering, and the associated losses in image resolution, implies that caution should be taken in interpreting fluid changes over time in areas of free convection.

Optimisation of Electrode Locations

For a uniform half-space, or when the associated inverse problem is linear, optimal survey design can be determined through an inverse modelling approach (Curtis, 1999a, b; Curtis and Maurer, 2000). Studies of experimental design for a homogenous half-space suggest that if all areas of the image plane are of equal interest, then the addition of surface electrodes and a reduction in electrode separation with depth, can improve resolution and decrease the number of measurement nodes required (Curtis and Maurer, 2000).

Figure 4 shows schematically the density of current "ray paths" in a uniform half-space for different electrode configurations; borehole-to-surface (current paths that pass from borehole electrodes to surface electrodes), borehole-to-borehole (current paths that pass from electrodes in one borehole to the electrodes in the other borehole), and a combined set-up that used borehole-to-borehole with borehole-to-surface electrodes (all possible combinations running from borehole to borehole and from each borehole to the surface). In regions of low or no current density, there is low resolution obtained and hence a poorly constrained inversion. Higher current density passing through an area results in better coverage and therefore a better-constrained inversion is possible.

Resolution is also affected by the grid employed, the orientation of the conductive bodies and the resistivity contrasts. In these studies, the mesh has a fine discretisation in all regions of the model between the boreholes, but the smoothness constraint maintains continuity of structure. We note that for diffusive flow of saline water into fresher groundwater, the resistivity contrasts will be small and will be smoothly varying over a broad volume due to mixing. Thus, we do not expect to have considerable variations in current density in the modelled area, and the optimisation studies in Figure 4 are generally appropriate.

Current density decreases with increasing distance from the current source, leading to less coverage towards the centre of the image plane (Slater et al., 1997) (Figure 4b). Dependency of current flow on resistivity structure also results in the current paths being non-linear, so that the actual current density at any one site will change in accordance with conductive or resistive bodies as well as with distance from the current source. Loss of resolution centrally can be reduced by ensuring that the interval between boreholes is no more than three quarters of the borehole depth, and ideally about half the borehole depth. However, addition of surface electrodes can assist with resolution for large borehole separations (Figure 4c) (LaBrecque et al., 1996a).

Sullivan and LaBrecque (1998) compared ERT images created by pole–pole surveys with those created by bipole–bipole surveys of varying separation, both with and without surface electrodes. They concluded that surface electrodes improved the resolution of upper layers, while pole–pole and the widest bipole–bipole spacing surveys showed the best overall resolution. Smaller electrode separations provided information on small-scale structures near the borehole, while losing resolution centrally. The combination of multiple ERT surveys with varying electrode separations across the target region can improve the overall resolution of images.

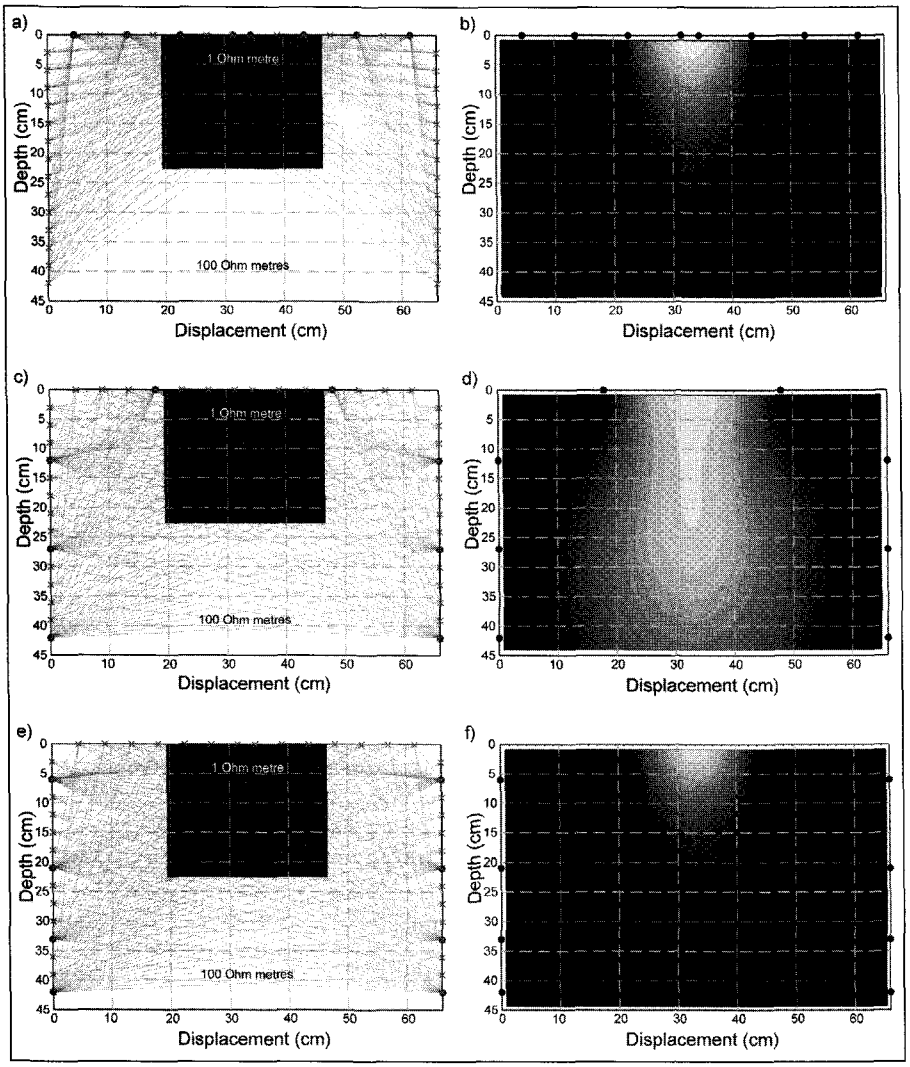

Fig. 5. A simple conductive rectangle of 1 Ω.m in a half space of 100 Ω.m was modelled using different electrode arrays. Eight current electrodes are used with 42 potential measurement sites. Schematic current paths are shown on the left whilst the ERT images are shown on the right with conductive areas light colours and resistive areas dark colours. A surface-only configuration (a and b), combined surface and borehole configuration (c and d), and borehole-only configuration (e and f) were modelled.

Three different models were created to examine electrode optimisation in Figure 5. These models again measured the potential at 42 sites, but only utilised eight current source sites, to conform to the electrode arrays required for the laboratory experiments. In Figure 5a, the current sources are at the surface; in Figure 5c three current electrodes are down hole, and one on the surface; and in Figure 5e all the current sources are down hole. Resolution of the plume is highly dependent on electrode location. Definition of the base of the plume for the surface current electrodes (Figure 5a and 5b) and the borehole current electrodes (Figure 5e and 5f) was comparable. Spreading current sources along the surface and down hole produced the best-resolved image of the plume.

LABORATORY INVESTIGATIONS

Figure 6 shows the narrow modelling tank that was utilised to approximate a quasi two-dimensional flow regime (Simmons et al., 2002). Two large glass panels (1200 x 600 mm) enable visual inspection of plume development. Base and sides of the tank were metal, which although not ideal for electrical experiments, was required for structural integrity. To minimise the effect of the metal edges, all experiments were conducted in the centre of the tank, with the electrodes 270 mm away from the sides, and the bottom electrode 180 mm from the base metal plate. Numerical models showed that while these metal edges lowered the overall resistivity, the relative effects were negligible and did not affect the delineation of a conductive plume. Although the tank is small, the dimensions of the cross-borehole space (approx. 600 mm by 600 mm) can be scaled up to real-world situations (boreholes 20+ m deep, separated by tens of metres). The utility of tank measurements is in the control of input parameters in order to provide greater confidence for field measurement interpretation.

The tank was filled with 18/40 grade sand (Commercial Minerals Ltd, Jolimont, Victoria) forming a porous subsurface. No attempt to layer or pack the sand was made when filling the tank, to approximate a homogenous environment. Simmons et al. (2002) conducted various tests on this type of sand, concluding that it had a normal grain-size distribution with a median grain size of 0.47 mm and with 99% of the grains in the range of 0.25–0.71 mm. A uniformity coefficient (D_{60}/D_{10} – the ratio of mass of grains that have passed through a size 60 sieve with a diameter of 0.250 mm to the mass that has passed through a size 10 sieve with a diameter of 2 mm) of 1.75 was

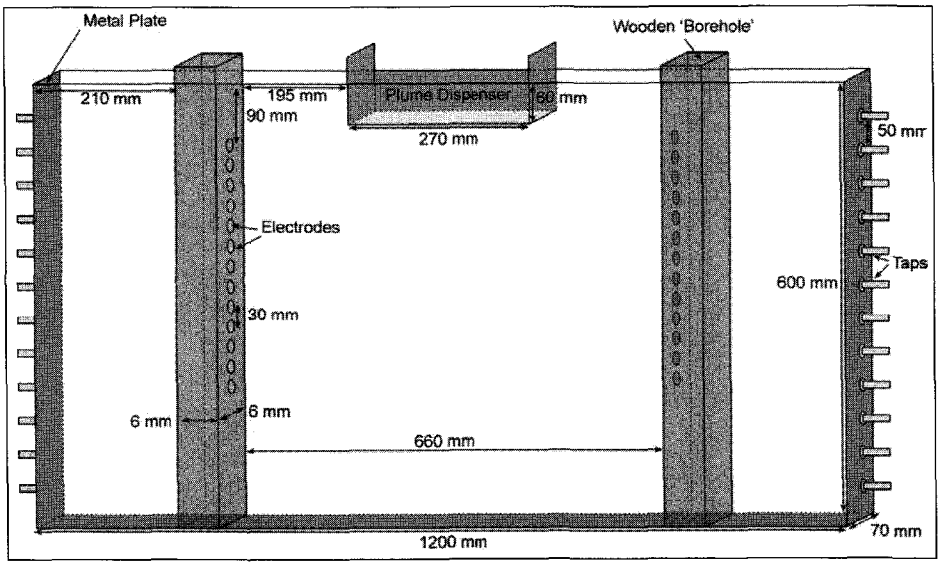

Fig. 6. Modelling tank. The two large faces are glass whiles the grey sides are metal plate.

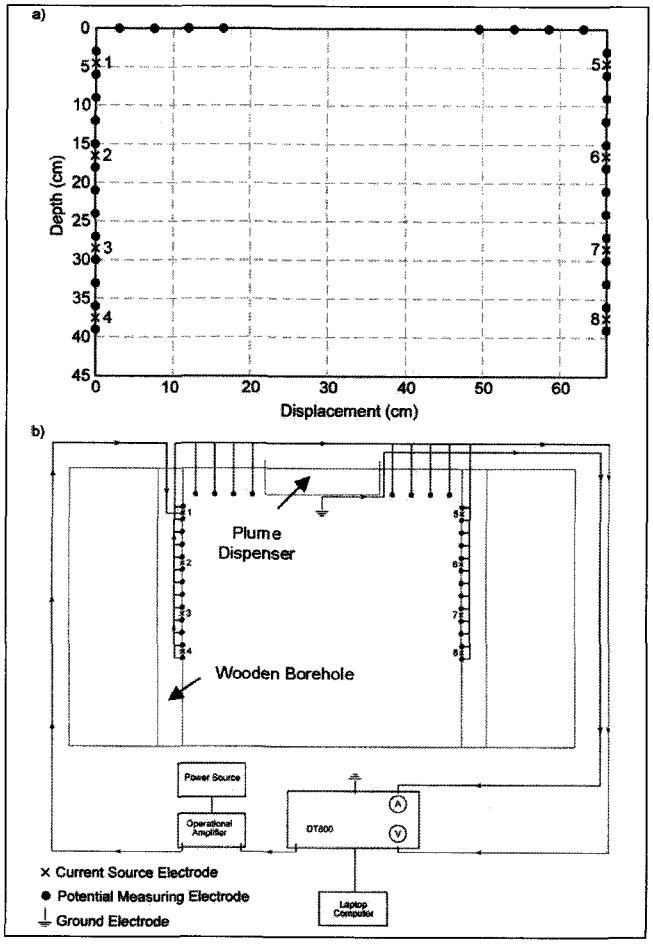

Fig. 7. (a) The positions of the electrodes for the laboratory experiment relative to the height at which the plume enters the tank (electrode positions are measured from the base of the plume dispenser).
(b) The ERT design, with the current passing from the Dater Taker DT800 through the externally powered operational amplifier to the first of the eight current electrodes. The resulting potential difference is then measured six times per second at all potential-measurement electrodes. These measurements are made simultaneously for all the electrodes by the DT800 and captured to disk on a laptop computer. The current passing through the ground electrode is measured twice per second, also by the DT8000.

determined and porosity after packing was 36%. Various hydraulic tests were conducted with a resultant average hydraulic conductivity of ~10^2 m/day.

Before commencing each experiment, the tank was flushed with desalinised water with a conductivity of less then 0.002 S/m, equivalent to a resistivity of more than 500 Ω.m. An electrical conductivity (EC) meter was used to continuously monitor the conductivity of the flushed liquid with experiments beginning once conductivity was less than 0.005 S/m (resistivity greater than 200 Ω.m). Once this threshold was reached, the water level was allowed to settle for a minimum of 15 minutes. Following this stage, the two taps, second from the top on both sides, were opened to create a static water level and again the water was allowed to settle, this time for a minimum of 60 minutes before the commencement of the experiment.

Figure 7 shows the electrode locations and ERT equipment, which consists of a DataTaker DT800 multiplexer, a power amplifier, a laptop computer, two wooden 'boreholes', eight current source electrodes, 34 electrodes to measure the potential, and a grounded 'sink' electrode. Cylindrical brass electrodes, approximately 50 mm long with a diameter of 8 mm were used for transmitting the current into the subsurface, and $Cu/CuSO_4$ electrodes in small porous pots, approximately 70 mm long and 2 mm in diameter were used to record potentials. The layout was based on results of numerical modelling that revealed that this configuration best resolved a simple plume (Figure 5). Positioning of down-hole electrodes was adapted to equipment limitations that prohibited the same electrode being used as a current source and for potential measurements, which also prohibited the creation of reciprocity measurements to test noise levels. A centrally located electrode (Figure 7b) was used as both the current sink and a reference for the potential measurements.

A low-frequency square wave current with a period of six seconds was used; voltages were sampled at 34 sites simultaneously at a rate of 6 Hz, so that in each cycle approximately 18 measurements were made while current was flowing, and a good average could be obtained. A reverse-polarity wave could not be generated by the DT800, but a three-second 'off' time was used to minimise any induced potential effects, and allow measurement of the self-potential (SP) effects. Five cycles were completed at each current electrode site before moving the current source to a different position. Thus, measurements from each current source took 30 seconds, and the duration of the entire, cycle (all combinations of current electrode sites) was completed in approximately four minutes.

Two experiments were conducted with a dense solution of calcium chloride ($CaCl_2$) to investigate complexity of free convective flow. Solutions of 300 000 mg/L (resistivity of 0.05 Ω.m), and 60 000 mg/L $CaCl_2$ (resistivity of 0.25 Ω.m) were used, with respective densities of 1.235 g/cm^3 and 1.048 g/cm^3. These solutions were stained with 1 ml/L Rhodamine-WT (20% active), a water-soluble tracer that is non-sorbing, non-degrading, relatively inert, and does not react with chloride. The tank was fully saturated for these experiments, with a water level maintained 7 cm below the top of the tank. The saline solutions were introduced at a rate of 500 ml every 4 minutes for 20 minutes, through a plastic rectangular box, measuring 270 mm long, 50 mm wide and 50 mm deep (as shown in Figure 6) and with a perforated galvanised iron base that enabled the fluid to pass through and be dispersed along a wider front than could be otherwise obtained.

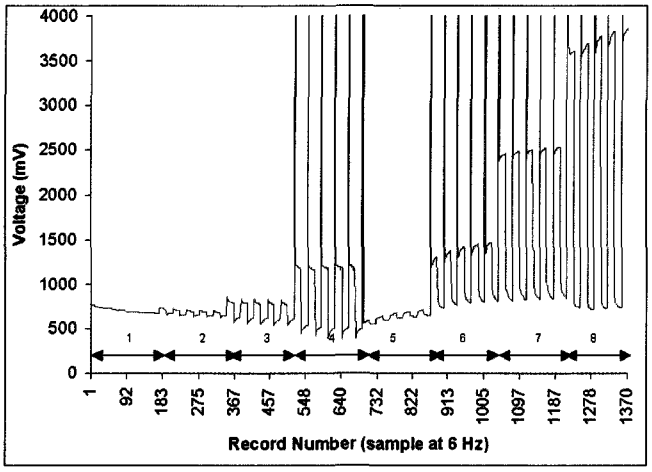

Fig. 8. Voltages at the bottom electrode in the right hand borehole, prior to the introduction of the plume, for an input square wave of period six seconds from current electrodes at each of the eight locations in Figure 7. A change of current electrode site is marked by a change in the amplitude of the measured voltages. The time axis ranges from 0 seconds to 240 seconds, a full sequence of five cycles at each current electrode site for all eight current electrodes.

Figure 8 shows a record of the voltages, before processing, measured at the bottom electrode in the right borehole. The order of energising of current electrodes one to eight respectively is from top to bottom in the left borehole, followed by top to bottom in the right borehole. Each transmission is of five square waves before changing the source of the current, and these intervals are marked on the figure. Raw data have spikes at the beginning of many of the "on" periods, most probably due to instrumentation noise. The largest potentials naturally occur when current sources were closest, in the same borehole as the potential electrode. Such measurements dominated the inversions and tended to created conductive edge anomalies; therefore, only cross-path measurements were used in the inversions.

A visual (photographic) record of a typical plume development is shown in Figure 9 for the 60 000 mg/L $CaCl_2$ plume, showing clearly the development of fingering in free convective flow. Images are photographed twelve minutes apart, and the major body of the plume is labelled A. Smaller plumes B and C are fingering effects.

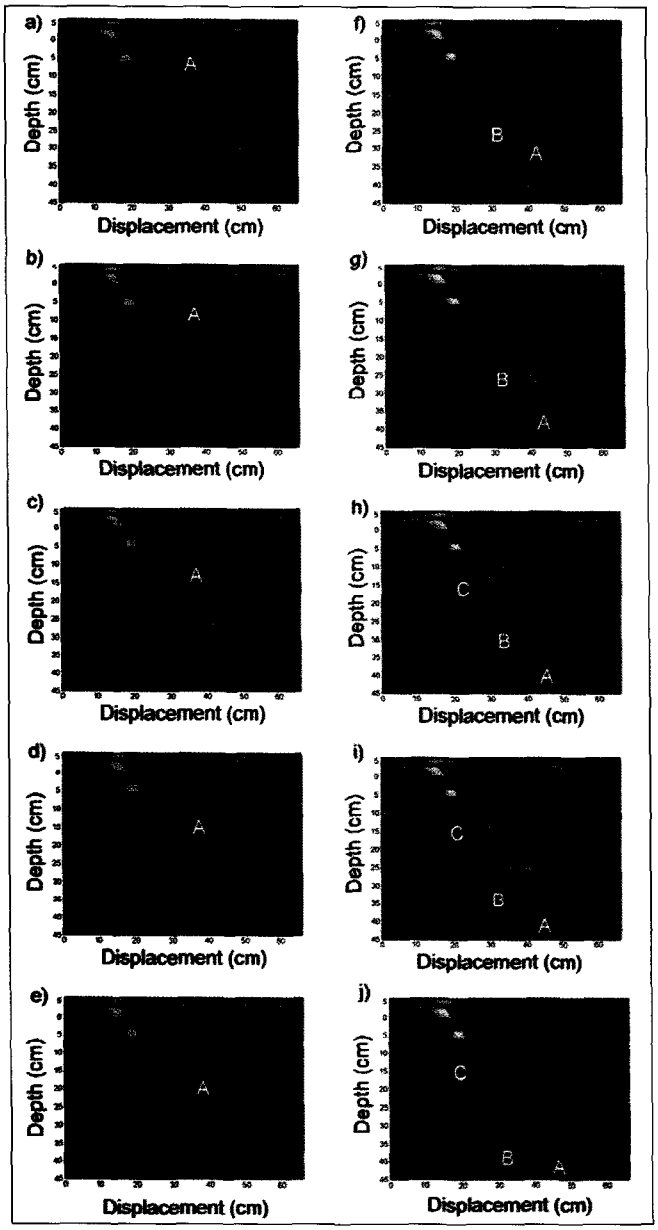

Fig. 9. Development of the 60 000 mg/L $CaCl_2$ plume over time. Images are twelve minutes apart, beginning at (a) on the left side and progressing alphabetically to (j). The major body of the plume is labelled A; B and C are fingering effects.

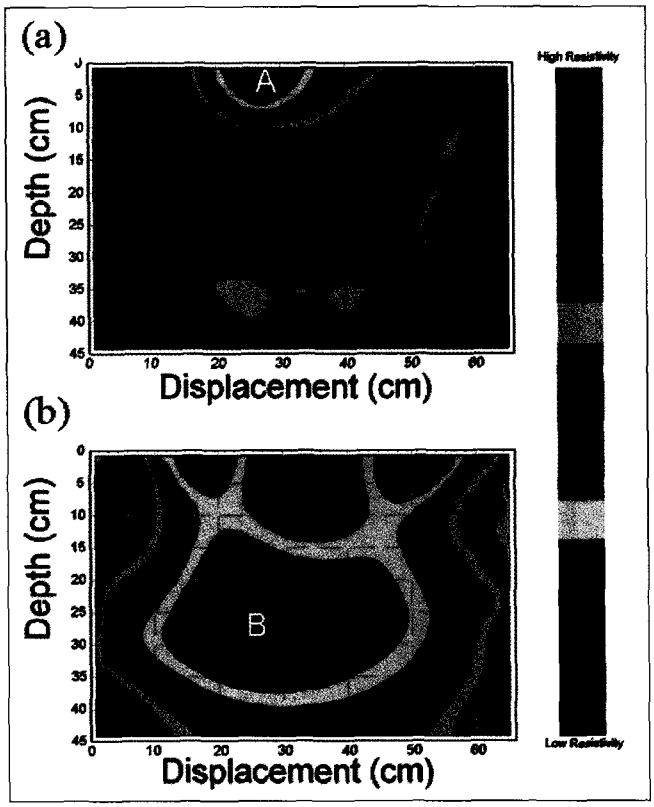

Fig. 10. ERT resistivity images of a 300 000 mg/L $CaCl_2$ solution plume development at (a) 12 minutes (compare with Figure 9b) and (b) 24 minutes after the introduction of the saline solution (compare with Figure 9d). The plume is imaged slightly deeper due to the greater density of the solute used in this run, and from heterogeneities in the tank sands that allow fluids to flow non-uniformly through the tank width.

Two-dimensional ERT inversions were created at twelve-minute intervals for the 300 000 mg/L $CaCl_2$ plume development, as shown in Figure 10. A photograph taken soon after the introduction of the solution in Figure 10a (comparable to Figure 9b) shows a small area of solute with no free convection effects labelled A. This same area is well resolved in the ERT image of Figure 10b (comparable to Figure 9d). We note that the ERT method images broad-scale resistivity changes (Plume A), but lacks resolution of fingering effects (Plumes B and C), as was determined from the numerical studies in Figure 3.

CONCLUSIONS

Numerical modelling showed that while ERT methods may image simple plume shapes, it would not resolve smaller-scale, mostly vertical fingering effects. Denser arrays and/or closer borehole spacings improve resolution, and it was found that optimisation of electrode locations may appreciably enhance the methodology. Comparisons of different survey designs determined that down-hole current sources together with a combination of borehole and surface potential measurement sites were better than surface-only or borehole-only configurations.

Laboratory modelling of high-density free convective flow was reasonably successful but questions remain as to whether the visual images are representative of the entire flow. It was noted during the experiments that flow paths were different on alternative sides of the tank, indicating that the flow is not truly consistent with any single photograph. We also note that the

modelling implied a two-dimensional resistivity structure with infinite strike; this was not the case, and current densities clearly increase within the tank. No fingering effects were resolved, and the depth to which these fingers penetrate is also in question. Improvements can be made to the ERT system used in this survey. A higher frequency wave could be used to increase temporal resolution and could potentially be used for additional induced polarisation (IP) and self-potential SP measurements. A denser array of electrodes and optimisation of location also would improve the resolution.

ACKNOWLEDGEMENTS

Financial support for this project was kindly provided by the Co-operative Centre for Landscapes Environment and Mineral Exploration, the Australian Society of Exploration Geophysicists Research Foundation, and the University of Adelaide. The authors thank Craig Simmons, Stewart Greenhalgh, Todd Halihan and Leslie McCluskey for their assistance with this research.

REFERENCES

Atekwana, E. A., Sauck, W.A., Abdel Aal, G.Z., and Werkema, D.D. Jr., 2002, Geophysical investigation of vadose zone conductivity anomalies at a hydrocarbon contaminated site: implications for the assessment of intrinsic bioremediation: *Journal of Environmental and Engineering Geophysics*, **7**, 103–110.

Barrett, B., Heinson, G., Hatch, M., and Telfer, A., 2002, Geophysical methods in saline groundwater studies: locating perched water tables and fresh-water lenses: *Exploration Geophysics*, **33**, 151–121.

Bevc, D., and Morrison, H.F, 1991, Borehole-to surface electrical resistivity monitoring of a salt water injection experiment: *Geophysics*, **56**, 769–777.

Chambers, J.E., Ogilvy, R.D., Meldrum, P.I., and Nissen, J., 1999, 3D resistivity imaging of buried oil and tar contaminated waste deposits: *European Journal of Environmental and Engineering Geophysics*, **4**, 1–13.

Curtis, A., 1999a, Optimal experiment design: cross-borehole tomographic examples: *Geophysical Journal International*, **136**, 637–650.

Curtis, A., 1999b, Optimal design of focused experiments and surveys: *Geophysical Journal International*, **139**, 205–215.

Curtis, A., and Maurer, H., 2000, Optimizing the design of geophysical experiments: Is it worthwhile?: *The Leading Edge*, **19**, 1058–1062.

Daily, W., and Owen, E., 1991, Cross-borehole resistivity tomography: *Geophysics*, **56**, 1228–1235.

Daily, W., Ramirez, A., LaBrecque, D., and Barber, W., 1995, Electrical resistance tomography experiments at the Oregon Graduate Institute: *Journal of Applied Geophysics*, **33**, 227–237.

Frind, E.O., 1982, Simulation of long term density-dependent transport in groundwater: *Advanced Water Resources*, **5**, 73–97.

Frohlich, R.K., and Urish, D.W., 2002, The use of geoelectrics and test wells for the assessment of groundwater quality of a coastal industrial site: *Journal of Applied Geophysics*, **50**, 261–278.

Granato, G.E., and Smith, K.P., 1999, Robowell: An automated process for monitoring ground water quality using established sampling protocols: *Ground Water Monitoring and Remediation*, **18**, 81–89.

Hassanizadeh, S.M., and Leijnse, T., 1988, On the modelling of brine transport in porous media: *Water Resources Research*, **24**, 321–330.

Huyakorn, P.S., Andersen, P.F., Mercer, J.W., and White, H.O., 1987, Saltwater intrusion in aquifers: development and testing of a three-dimensional finite element model: *Water Resources Research*, **23**, 293–312.

Johnson, V.M., Tuckfield, R.C., Ridley, M.N., and Anderson, R.A., 1996, Reducing the sampling frequency of groundwater monitoring wells: *Environmental Science and Technology*, **30**, 355–358.

LaBrecque, D. J., 1989, *Cross-borehole resistivity modelling and model fitting*: PhD Thesis, University of Utah.

LaBrecque, D. J., Ramirez, A. L., Daily, W. D., Binley, A. M. and Schima, S. A., 1996a, ERT monitoring of environmental remediation processes: *Measurement Science and Technology*, **7**, 375–383.

LaBrecque, D.J. Miletto, M., Daily, W., Ramirez, A., and Owen, E., 1996b, The effects of noise on Occam's inversion of resistivity tomography data: *Geophysics*, **61**, 538–548.

LaBrecque, D., and Ward, S., 1998, Two-dimensional inversion of cross-borehole resistivity data using multiple boundaries: *58th Annual International Meeting, Society of Exploration Geophysics, Extended Abstracts*, 194–197.

Loke, M.H., and Barker, R.D., 1996a, Rapid least-squares inversion of apparent resistivity pseudosections by a quasi-Newton method: *Geophysical Prospecting*, **44**, 131–152

Loke, M.H., and Barker, R.D., 1996b, Practical techniques for 3D resistivity surveys and data inversion: *Geophysical Prospecting*, **44**, 499–523

Newmark, R.L., Daily, W.D., Kyle, K.R., and Ramirez, A. L., 1998, Monitoring DNAPL pumping using integrated geophysical techniques: *Journal of Environmental and Engineering Geophysics*, **3**, 7–13.

Nobes, D.C., 1996, Troubled waters: Environmental applications of electrical and electromagnetic methods: *Surveys in Geophysics*, **17**, 393–454.

Ogilvy, R.D., Meldrum, P.I., and Chambers, J.E., 1999, Imaging of industrial waste deposits and buried quarry geometry by 3D resistivity tomography: *European Journal of Environmental and Engineering Geophysics*, **3**, 103–113.

Oostrom, M., Dane, J.H., Güven, O., and Hayworth, J.S., 1992, Experimental investigation of dense solute plumes in an unconfined aquifer model: *Water Resources Research*, **28**, 2315–2326.

Ramirez, A., Daily, W., LaBrecque, D., Owen, E., and Chesnut, D., 1993, Monitoring underground steam injection process using electrical resistance tomography: *Water Resources Research*, **29**, 73–87.

Slater, L.D., Binley, A., and Brown, D., 1997, Electrical imaging of fractures using groundwater salinity change: *Ground Water*, **35**, 436–442.

Simmons, C.T., and Narayan, K.A., 1998, Modelling density-dependent flow and solute transport at the Lake Tutchewop saline disposal complex, Victoria: *Journal of Hydrology*, **206**, 219–236.

Simmons, C.T., Pierini, M.L., and Hutson, J.L., 2002, Laboratory investigation of variable-density flow and solute transport in unsaturated-saturated porous media: *Transport in Porous Media*, **47**, 215–244.

Sullivan, E., and LaBrecque, D., 1998, Optimization of ERT Surveys: *Proceedings of the Symposium on the Application of geophysics to environmental and engineering problems (SAGEEP)*, 571–581.

Tripp, A.C., Hohmann, G.W., and Swift, C.M. Jr, 1984, Two dimensional resistivity inversion: *Geophysics*, **49**, 1708–1717.

Zhou, Y., 1996, Sampling frequency for monitoring the actual state of ground water systems: *Journal of Hydrology*, **180**, 301–318.

Zhou, B., and Greenhalgh, S.A., 1997, A synthetic study on crosshole resistivity imaging with different electrode arrays: *Exploration Geophysics*, **28**, 1–5.

Zhou, B., and Greenhalgh, S.A., 1999, Explicit expressions and numerical computation for the Fréchet and second derivatives in 2.5-D Helmholtz equation inversion: *Geophysical Prospecting*, **48**, 443–468.

Zhou, B., and Greenhalgh, S.A., 2000, Crosshole resistivity tomography using different electrode configuration: *Geophysical Prospecting*, **48**, 887–912.